

Interatomic and intermolecular Coulombic decay rates from equation-of-motion coupled-cluster theory with complex basis functions

Valentina Parravicini¹ and Thomas-C. Jagau¹
Department of Chemistry, KU Leuven, B-3001 Leuven, Belgium

When a vacancy is created in an inner-valence orbital of a dimer of atoms or molecules, the resulting species can undergo interatomic/intermolecular Coulombic decay (ICD): the hole is filled through a relaxation process that leads to a doubly ionized cluster with two positively charged atoms or molecules. Since they are subject to electronic decay, inner-valence ionized states are not bound states but electronic resonances whose transient nature can only be described with special quantum-chemical methods. In this work, we explore the capacity of equation-of-motion coupled-cluster theory combined with two techniques from non-Hermitian quantum mechanics, complex basis functions and Feshbach-Fano projection, to describe ICD. To this end, we compute decay rates of several dimers: Ne₂, NeAr, NeMg, and (HF)₂, among which the energy of the outgoing electron varies between 0.3 eV and 16 eV. We observe that both methods deliver better results when the outgoing electron is fast, but the characteristic R^{-6} distance dependence of the ICD width is captured much better with complex basis functions.

I. INTRODUCTION

Interatomic/intermolecular Coulombic decay (ICD)^{1,2} is a very efficient non-radiative relaxation process that occurs in atomic and molecular clusters. When a vacancy has been created in an inner-valence orbital, non-radiative intramolecular relaxation, such as Auger-Meitner decay^{3,4} (Fig. 1a) cannot take place as it is energetically forbidden. The relaxation of the atom or molecule can, however, lead to the ionization of a neighbour. This mechanism is allowed when the lowest double ionization energy of the cluster is lower than the ionization energy that was needed to create the vacancy. This is the case for inner-valence orbitals, while outer-valence orbitals do not have enough energy to relax via this process. We note, however, that the distinction between inner-valence orbitals and outer-valence orbitals is not as obvious as between core and valence orbitals of light atoms. Rather, one has to compute the relevant energies explicitly to see if ICD is possible.

ICD happens via two different mechanisms, referred to as direct and exchange.⁵ The former (Fig. 1b) consists in an energy transfer process, while the latter (Fig. 1c) is mediated by the exchange of an electron between the two partners. For clusters of rare gas atoms, it has been argued that the direct contribution is more relevant because orbital overlap is small in those cases. The direct contribution is the one that is responsible for the characteristic distance dependence of the decay width of ICD, that is, R^{-6} with R being the interatomic distance. This result is obtained by expanding the relevant two-electron repulsion integral in an inverse power series in R .^{6,7} The exchange contribution instead decays more rapidly with an exponential dependence on R as the two partners are moved apart because it is driven by orbital overlap.

Typical ICD lifetimes are of the order of tens or hundreds of femtoseconds. ICD outperforms radiative decay pathways like photon emission, which usually takes place on the nanosecond scale, and is competitive with nuclear dynamics. Compared to Auger decay, however, ICD happens on a longer timescale; the former process typically has lifetimes of a few femtoseconds. For this reason, ICD widths are smaller than Auger decay widths. Also, ICD lifetimes have been proven to be strongly affected by environmental factors, for example,

the presence of other neighbouring species^{8,9}, their number and their structure.¹⁰⁻¹⁴

Similar to Auger decay, we can identify different doubly ionized states into which the initial inner-valence ionized state can decay. We will refer to them as target or final states. The energy differences between initial and final states are identical to the energy of the outgoing electron, which typically is in the range of 0–20 eV for ICD. This means that ICD electrons are at least one order of magnitude slower than Auger electrons, which usually have energies of hundreds of eV for first-row nuclei or even thousands of eV in the case of heavier nuclei.

Closely related to ICD is electron transfer mediated decay¹⁵ (ETMD), where the relaxation of an inner-valence vacancy results in a doubly ionized neighbour (Fig. 1d). This process is allowed when the ionized atom has a neighbour with a double ionization energy lower than the ionization energy associated with the initial vacancy. ETMD is slower than ICD and only becomes relevant at very short internuclear distances. In fact, since ETMD is driven by orbital overlap, the decay width decreases with distance in the same way as the exchange term of ICD, that is, as e^{-R} .

Owing to their instability towards electron loss, inner-valence ionized states can be categorized as electronic resonances.¹⁶⁻¹⁸ These states are not L^2 -integrable and cannot be tackled with quantum-chemical methods suitable for bound states unless the decay is ignored. However, several methods have been devised to extend bound-state methods to capture the transient nature of resonances. In the framework of non-Hermitian quantum mechanics,¹⁶ the energy of resonances is expressed as

$$E_{\text{res}} = E_R - i\Gamma/2, \quad (1)$$

where E_R is the real part of the energy, also called the position of the resonance, and Γ its decay width, related to the lifetime as $\tau = 1/\Gamma$.

Several approaches have been introduced for the *ab initio* computation of ICD and ETMD widths. In Feshbach-Fano resonance theory,^{19,20} the outgoing electron is modeled explicitly or, alternatively, Stieltjes imaging²¹ is employed. The latter approach has been employed in conjunction with algebraic diagrammatic construction^{5,22,23} (ADC) and configura-

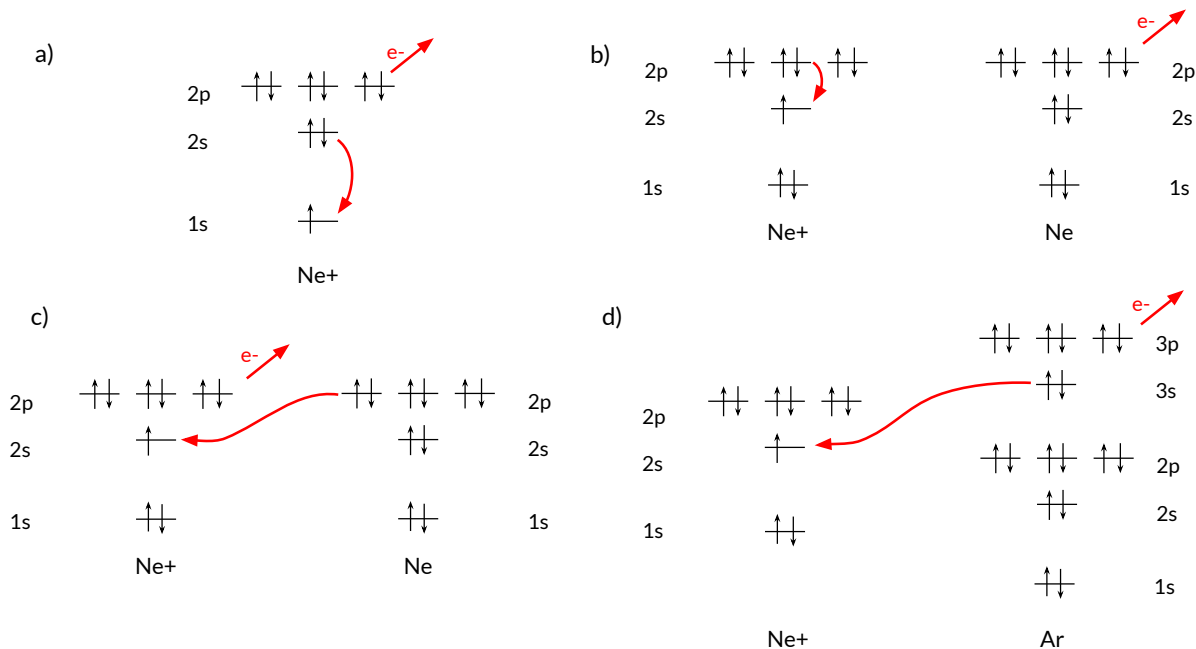


FIG. 1. Schematic representation of non-radiative decay processes of core-ionized and inner-valence ionized species: a) Auger decay b) ICD – direct term c) ICD – exchange term d) ETMD

tion interaction²⁴ (CI). Other options are R-matrix theory²⁵ and complex adsorbing potentials^{26–28} (CAPs), which decouple the resonance from the continuum and make it square-integrable.

In this work, we explore the performance of two further non-Hermitian techniques for ICD widths. These are Feshbach-Fano resonance theory^{19,20} with a plane-wave description for the outgoing electron²⁹ and the method of complex basis functions³⁰ (CBFs). We combine both techniques with equation-of-motion coupled-cluster singles and doubles (EOM-CCSD) and investigate ICD in the dimers Ne_2 , NeAr , NeMg , and $(\text{HF})_2$. EOM-CCSD^{31,32} is a powerful *ab initio* electronic-structure method to describe various types of excited states. In this work, we employ its ionization potential variant³³ (EOM-IP-CCSD) to describe the initial states of ICD and its double ionization variant (EOM-DIP-CCSD) to describe the final states.^{34,35} The CBF method has already been successfully employed to describe various other types of electronic resonances, such as temporary anions^{30,36–42} and molecules in strong electric fields.^{43–46} Recently, CBFs combined with EOM-CCSD and CCSD were applied to molecular Auger decay.^{47–49} The combination of Feshbach-Fano theory with EOM-CCSD and an explicit representation of the outgoing electron has also been employed to compute molecular Auger decay widths.^{29,49,50}

The remainder of the article is structured as follows: Sec. II summarizes the computational methods, while Secs. III–VI present our numerical results for Ne_2 , NeAr , NeMg , and $(\text{HF})_2$, respectively. In Sec. VII we give our general conclusions.

II. THEORETICAL AND COMPUTATIONAL DETAILS

A. Method of complex basis functions

The CBF method³⁰ is a variant of complex scaling^{16,51,52} that is compatible with the Born-Oppenheimer approximation, and thus suitable for molecules. The two are related through the equation

$$E_{\text{res}} = \frac{\langle \Psi(r) | \hat{H}(re^{i\theta}) | \Psi(r) \rangle}{\langle \Psi(r) | \Psi(r) \rangle} = \frac{\langle \Psi(re^{-i\theta}) | \hat{H}(r) | \Psi(re^{-i\theta}) \rangle}{\langle \Psi(re^{-i\theta}) | \Psi(re^{-i\theta}) \rangle} \quad (2)$$

where the complex scaling angle θ can assume values between 0 and $\pi/4$. In the CBF method, the complex-scaled wave function is expressed in terms of basis functions with scaled exponents, as in the context of Gaussian functions scaling the exponent is asymptotically equivalent to scaling the coordinates. Additional flexibility results from the fact that not all but only some functions in a basis set need to be scaled. A Hamiltonian built in such a basis set will have complex-valued eigenvalues that can be interpreted in terms of Eq. (1).

Recently, it was shown that Auger decay widths can be treated with CBF versions of EOM-IP-CCSD and CCSD.^{47,48} The CCSD approach, which is based on a Hartree-Fock (HF) determinant for the decaying state is, however, not viable in the case of ICD. While it is, in general, no problem to construct a HF wave function with a hole in an inner-valence orbital using root-following techniques,⁵³ the CCSD wave function built from such a determinant suffers from variational collapse because the hole in the inner-valence shell is close

in energy to occupied orbitals. This is different from core-ionized states, where the energetic separation between core and valence orbitals prevents a variational collapse. EOM-IP-CCSD does not suffer from such a problem because the HF and CCSD equations are solved for the neutral ground state.

Unless specified otherwise, the basis set employed for all CBF calculations is aug-cc-pCVTZ(5sp): in this basis set, the triple ζ basis is modified by substituting the s and p shells with those from aug-cc-pCV5Z. It has been shown that this basis is suitable for the description of Auger decay.⁴⁷ When extra shells are added on top of aug-cc-pCVTZ(5sp), their exponents are obtained by recursively dividing the most diffuse exponent by a factor of 2, unless explicitly stated otherwise.

As concerns the exponents of the complex-scaled shells, it has been suggested that their value is related to the energy of the outgoing electron.⁴⁷ For the description of Auger electrons with a few hundreds of eV, one needs to scale shells with exponents in the range of 1–10, whereas diffuse shells are needed for temporary anions where the outgoing electron at most has a few eV. Consequently, for ICD, where electron energies are roughly in the same range as for temporary anions, we also expect diffuse complex-scaled shells to be important.

This is investigated in detail for the Ne₂ dimer in Sec. III B. For other atoms, the exponents of the complex-scaled shells are adapted from neon according to the method from Ref. 47: a diffuseness factor f is calculated for each atom, and the exponents (ζ) for the new atom are calculated as $\zeta_2 = \zeta_1 \cdot f_2/f_1$. These factors are 6.36, 4.23, 1.34, 0.41, 4.28 for the aug-cc-pCVTZ(5sp) basis sets of Ne, Ar, Mg, H and F, respectively.

A technical complication of CBF calculations is that one has to find an optimal scaling angle. In the present work, we determine the angle by minimizing $d(E_{\text{res}} - E_0)/d\theta$,⁵⁴ where E_0 is the energy of the neutral ground state. This derivative is evaluated by recalculating the energy at different angles and numerical differentiation. The spacing between two angles is 2°, beside for the values reported in Table II, where the spacing is 1.5°.

All CBF-EOM-IP-CCSD calculations presented in this work were carried out using a developer’s version of the Q-Chem program package,⁵⁵ version 6.0. Details of the implementation are available from Refs. 40–42,56.

B. Feshbach-Fano projection method

In Feshbach-Fano theory,^{19,20} resonances are described by the interaction of a bound state and scattering-like continuum states. The two sorts of states are obtained by partitioning the Hilbert space by means of projection operators, which can take many forms as long as they respect the condition to be mutually orthogonal and sum up to 1.

Recently, Skomorowski and Krylov combined Feshbach-Fano theory with EOM-CCSD methods to describe Auger decay of core-ionized and core-excited states.^{29,50} In their approach, the bound part of the Hilbert space is defined using core-valence separation^{57–59} (CVS) and the continuum states are represented by products of EOM-CCSD states and a free-electron state, described by a continuum orbital.

In this work, we employ a similar approach to describe ICD. A generalized CVS scheme, where the “core” includes the inner-valence orbitals, is used to define the bound state. This state is decoupled from the continuum because the ICD final states are not included in the EOM-IP-CCSD excitation manifold. However, we note that the assumption underlying CVS, that core and valence orbitals can be treated separately, does not hold for inner-valence and outer-valence orbitals, as the energetic separation between them is usually just a few eVs or even less. The validity of this approach for treating ICD is thus questionable.

We represent the continuum states as products of EOM-DIP-CCSD states and free-electron states described by plane waves. We note that it has been demonstrated in the framework of Auger decay that the plane-wave approximation is better when the energy of the outgoing electron is high.²⁹ Since the energetic separation between initial and final states is much smaller for ICD than for Auger decay, the outgoing electron has much less energy, which again calls into question the validity of the approach.

All Feshbach-Fano-EOM-CCSD calculations presented in this work were carried out using a developer’s version of the Q-Chem program package,⁵⁵ version 6.0. Details of the implementation are available from Ref. 29. The basis set employed for all Feshbach-Fano-EOM-CCSD calculations is aug-cc-pCV5Z.

III. NEON DIMER

A. Energetics

The neon dimer has been investigated as a prototypical example of ICD in many works. Upon ionization of a 2s orbital, two states arise, $^2\Sigma_g^+$ and $^2\Sigma_u^+$, both of which can decay via ICD. At the equilibrium distance of neutral Ne₂ (3.2 Å) the inner-valence ionization energies are 48.369 eV for the $^2\Sigma_g^+$ state and 48.354 eV for the $^2\Sigma_u^+$ state, meaning the two resonances are only 15 meV apart. In Fig. 2, we report the ionization energies of the two states as a function of the interatomic distance. In the range considered (3.10–3.45 Å), the change is less than 20 meV but we observe that the energy difference between the two states slightly decreases from 19 meV to 6 meV as the atoms are moved apart.

We identified 12 possible ICD target states whose energies at the equilibrium distance are reported in Tab. I. We observe that all target states are close in energy spanning a range of less than 0.2 eV. Comparing the energy of initial and final states shows that the emitted ICD electron has an energy of less than 1 eV, which is in good agreement with previous theoretical⁶⁰ and experimental⁶¹ investigations that found the distribution of ICD electrons to peak at around 0.7 and 0.5 eV, respectively.

We also studied the distance dependence of the double ionization energies of the target states. All 12 states remain accessible via ICD in the range considered here but, contrary to the initial states, the double ionization energies decrease by

ca. 0.5 eV as the internuclear distance grows from 3.10 Å to 3.45 Å. This can be explained by the repulsion between the two positive charges being weaker when the two atoms are farther apart.

The target states can be divided into three groups of almost degenerate states. In Fig. 2 we report one state for each group, while the results for all states can be found in the Supplementary Material. The lowest-lying group comprises 6 states of Σ and Δ symmetry from Tab. I, while the middle group comprises 4 Π states and the highest-lying group 2 Σ states.

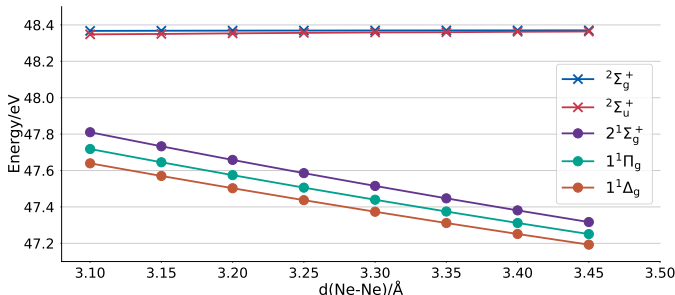


FIG. 2. Selected single and double ionization energies of Ne_2 as a function of the interatomic distance calculated with CBF-EOM-IP-CCSD/aug-cc-pCVTZ(5sp)+2s2p2d and EOM-DIP-CCSD/aug-cc-pCVTZ(5sp), respectively. Crosses correspond to resonances, thus initial states of ICD, and dots to final states of ICD.

TABLE I. Selected single and double ionization energies of Ne_2 computed with EOM-DIP-CCSD/aug-cc-pCVTZ(5sp)+2s2p2d at $R = 3.2$ Å. Only doubly ionized states accessible via ICD are reported.

Resonance state	Energy/eV	
$2\Sigma_g^+$	48.369	
$2\Sigma_u^+$	48.354	
Target state	Singlet/eV	Triplet/eV
$1\Delta_u$	47.502	
$1\Sigma_g^-$		47.502
$1\Delta_g$	47.503	
$1\Sigma_u^-$		47.503
$1\Sigma_g^+$	47.504	
$1\Sigma_u^+$		47.504
$1\Pi_g$	47.575	47.578
$1\Pi_u$	47.578	47.575
$2\Sigma_g^+$	47.658	
$2\Sigma_u^+$		47.658

B. ICD widths computed with complex basis functions

In Tab. II the total widths of the two states of Ne_2^+ calculated with CBF-EOM-IP-CCSD are reported. Several attempts were made, varying the size of the basis set and the number, angular momentum, and exponent of the complex-scaled functions. It can be observed that the widths of both states are very sensitive to the exponents of the complex-

scaled shells. This especially applies to the *ungerade* state whose decay width is most difficult to capture.

Contrary to temporary anions, adding scaled functions that are more diffuse than the unscaled ones already present in the aug-cc-pCVTZ basis set does not lead to a better description of the resonance state. Decay widths are uniformly too small, in some cases even negative. The results improve, especially for the $2\Sigma_g^+$ state, when we replace the s and p shells in the aug-cc-pCVTZ basis set with the ones from aug-cc-pCV5Z and scale the most diffuse shell of each angular momentum (s, p and d) in the resulting basis set. Adding new functions instead of scaling the ones already present in the basis set leads to further improvement. Notably, the exponents of the additional shells need not be smaller than the other exponents. This is somewhat similar to Auger decay even though the functions needed there have exponents in the range of 1–10.

As shown in Tab. III, the best match with other values computed at the same internuclear distance (3.2 Å) is obtained with exponents 0.5 and 0.08 for the two extra s, p and d shells. We also note a Fano-CI study that reported widths of 5.0 and 9.0 meV for the *gerade* and *ungerade* states, respectively, at $R=3.09$ Å employing a cc-pVQZ+7s7p7d basis set.²⁴ Also, the lifetime of the average of the two states was measured by means of a pump-probe experiment⁶² as (150 ± 50) fs, which corresponds to a width between 3.3 and 6.6 meV. It is, however, not possible to directly compare this latter value to computational results that do not take into account nuclear motion.

Starting from the best result in Tab. II, i.e., the values in the last row, we explored the sensitivity of the ICD widths to small changes in the exponents. Such an analysis had been performed for Auger decay⁴⁷ and it had been found that the optimal exponents are marked by concurrent minima in $\text{Im}(E_{\text{res}} - E_0)$ and $d(E_{\text{res}} - E_0)/d\theta$. This is reproduced in the top panel of Fig. 3. In the middle and lower panels of Fig. 3 we report the results of the corresponding analysis for the $2\Sigma_g^+$ and $2\Sigma_u^+$ states of Ne_2^+ . We varied the exponents of s, p, and d shells together; their values for each point are reported in the Supplementary Material. For each new basis set, the optimal complex-scaling angle was determined anew.

The stark difference between Auger decay and ICD is obvious in Fig. 3. While there are clear concurrent minima in both curves for Auger decay, the plots are a lot less neat for ICD. For the *gerade* state, there is a minimum in $\text{Im}(E)$ but this is not the case for the *ungerade* state. Moreover, the quantity $d(E_{\text{res}} - E_0)/d\theta$, which is used to find the optimal complex scaling angle, is not a good indicator of the quality of the exponents in the case of ICD. A possible explanation may be that the ICD widths of Ne_2^+ are at least one order of magnitude smaller than the Auger decay widths studied in Ref. 47.

The exponents that correspond to a minimum in $\text{Im}(E_{\text{res}} - E_0)$ for the $2\Sigma_g^+$ state are 0.889 and 0.143 and yield decay widths of 14.2 meV for the $2\Sigma_g^+$ state and 6.0 meV for the $2\Sigma_u^+$ state. This is markedly different from the widths of 10.1 and 7.6 meV obtained with the original exponents (0.5 and 0.08). The latter set of values is in better agreement with the other values compiled in Tab. III but a final decision which set of values is superior remains difficult. Notably, the two

TABLE II. Total decay widths Γ of the two $\text{Ne}_2^+(2s^{-1})$ states computed with CBF-EOM-IP-CCSD and various basis sets at $R = 3.2 \text{ \AA}$. Values in meV.

Basis set	Scaled basis functions	Exponents of the scaled functions	$^2\Sigma_g^+$	$^2\Sigma_u^+$
aug-cc-pCVTZ+2s2p	extra shells + most diff. spd shell of the predefined basis set	s (0.11, 0.57, 0.03) p (0.09, 0.04, 0.03) d (0.39)	0.4	0.6
aug-cc-pCVTZ+2s2p	extra shells	s (0.57, 0.03) p (0.04, 0.03)	-2.2	-0.4
aug-cc-pCVTZ+2s2p2d	extra shells	s (0.57, 0.03) p (0.04, 0.03) d (0.19, 0.10)	3.0	2.6
aug-cc-pCVTZ(5sp)	most diff. spd shell of the predefined basis set	s (0.10) p (0.06) d (0.39)	13.2	5.2
aug-cc-pCVTZ(5sp)	2 most diff. spd shell of the predefined basis set	s (0.29, 0.10) p (0.19, 0.06) d (1.10, 0.39)	2.6	0.4
aug-cc-pCVTZ(5sp)	3 most diff. spd shell of the predefined basis set	s (0.73, 0.29, 0.10) p (0.52, 0.19, 0.06) d (4.01, 1.10, 0.39)	6.6	2.4
aug-cc-pCVTZ(5sp)+2s2p2d	extra shells	1.0, 0.5	9.2	1.0
aug-cc-pCVTZ(5sp)+2s2p2d	extra shells	0.5, 0.2	11.6	1.6
aug-cc-pCVTZ(5sp)+2s2p2d	extra shells	0.2, 0.08	0.8	0.6
aug-cc-pCVTZ(5sp)+2s2p2d	extra shells	0.5, 0.08	10.1	7.6

TABLE III. Total decay width Γ of the two $\text{Ne}_2^+(2s^{-1})$ states computed with various electronic structure methods at $R = 3.2 \text{ \AA}$. An experimental value is also given. All values are in meV.

Method	$^2\Sigma_g^+$	$^2\Sigma_u^+$
CAP-CI/d-aug-cc-pVDZ +3s3p3d ²⁶		10.3
CAP-ADC(2)/d-aug-cc-pV5Z ²⁷		7.1
CAP-EOM-CCSD/aug-cc-pCVTZ+3s3p3d ¹²		7.2
CBF-EOM-IP-CCSD/aug-cc-pCVTZ(5sp)+2s2p2d (this work)	10.1	7.6
Feshbach-Fano-EOM-IP-CCSD/aug-cc-pCV5Z (this work)	8.2	7.3
Experimental value ⁶²	(150 ± 50) fs $\hat{=}$ 3.3–6.6 meV	

resonance states do not overlap with either set of Γ values as the energy gap between them (15 meV) is bigger than the sum of their half widths.

We also investigated the distance dependence of the width of both states, this was done using the exponents from the last row of Tab. II. The results are reported in Fig. 4. We see that the R^{-6} dependency is not captured correctly; rather, a log-log plot reveals that the width of the $^2\Sigma_g^+$ state decreases as R^{-12} and that of the $^2\Sigma_u^+$ as R^{-8} . Also, Fig. 4 illustrates again that the *ungerade* state is more difficult to describe than the *gerade* state. We note that Ghosh *et al.* also studied the distance dependence of width of the Σ_u^+ state using CAP-EOM-CCSD.¹² Our results are in good agreement at $R = 3.2 \text{ \AA}$ and larger distances, but when the two atoms are closer to each other, we obtain larger widths than the ones reported in Ref. 12.

C. ICD widths computed with the Feshbach-Fano method

As concerns Feshbach-Fano EOM-CCSD, we present ICD widths for Ne_2^+ computed at the equilibrium distance (3.2 \AA)

with various basis sets in Tab. IV. The width narrows as the basis set increases in size, and the value computed with aug-cc-pCV5Z compares well with the one obtained with CBF-EOM-IP-CCSD and previous computational results as one can see from Tab. III. However, as evident from Fig. 4, the method is not able to describe the distance dependence of the width correctly: instead of a decrease proportional to R^{-6} , we observe a linear trend for the $^2\Sigma_g^+$ state, whereas the width of the $^2\Sigma_u^+$ state even increases with the distance.

We conclude that the Feshbach-Fano EOM-CCSD method devised for Auger decay is not suitable for ICD. This failure is not surprising given the shortcomings discussed in Sec. II B: first, our Q projector for the bound part of the resonance is based on a generalization of CVS that does not hold for inner-valence orbitals as their energies are not well separated from the outer-valence orbitals. Moreover, we model the outgoing electron as a plane wave, which is an approximation that holds better when the energy of the outgoing electron is higher.

TABLE IV. Total decay width of the $\text{Ne}_2^+(2s^{-1})$ states calculated with Feshbach-Fano-EOM-CCSD with various basis sets. Values are in meV.

Basis set	$^2\Sigma_g^+$	$^2\Sigma_u^+$
aug-cc-pCVDZ	11.2	19.2
aug-cc-pCVTZ	9.2	12.3
aug-cc-pCVQZ	8.5	8.8
aug-cc-pCV5Z	8.2	7.3
aug-cc-pCVTZ(5sp)	9.1	11.3

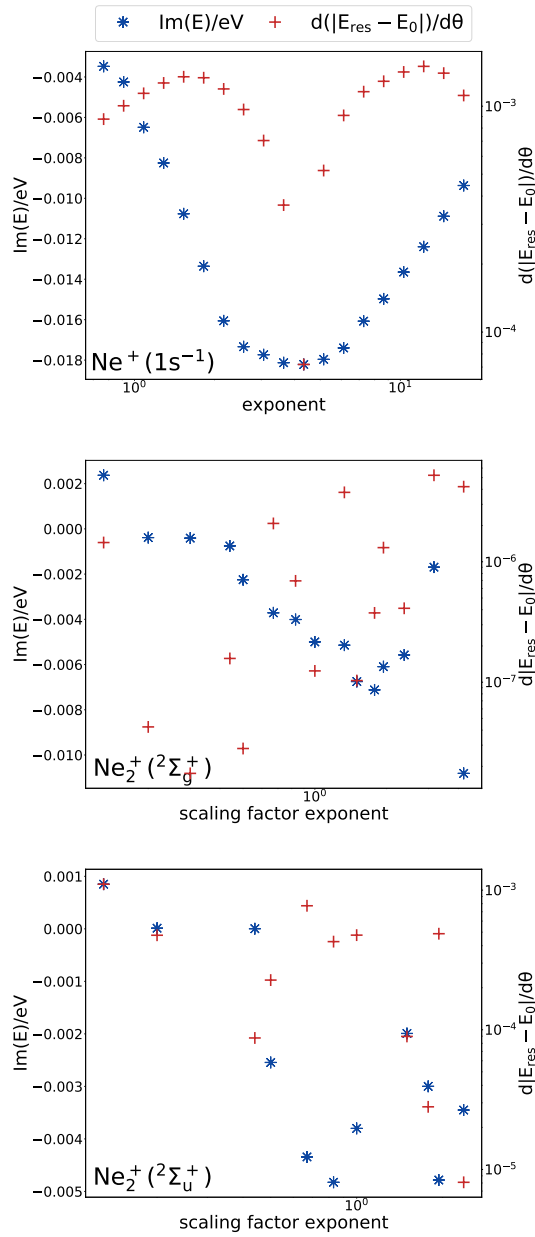


FIG. 3. Imaginary energy ($= -\Gamma/2$) and $d(E_{\text{res}} - E_0)/d\theta$ for the resonance states $\text{Ne}^+(1s^{-1})$ ⁴⁷, $\text{Ne}_2^+(2\Sigma_g^+)$ (this work) and $\text{Ne}_2^+(2\Sigma_u^+)$ (this work) as a function of the value of the exponents of the complex-scaled functions.

IV. NEON ARGON DIMER

A. Energetics

As a second example, we study the NeAr dimer. It has been demonstrated that NeAr can undergo both ICD and ETMD upon ionization of the 2s orbital of the neon atom.¹⁵ The two processes differ in the atoms that carry the vacancies in the final doubly ionized state: ICD results in Ne^+Ar^+ while in ETMD the two vacancies are found on Argon, NeAr^{2+} . Target states of the type Ne^{2+}Ar are higher in energy than the ini-

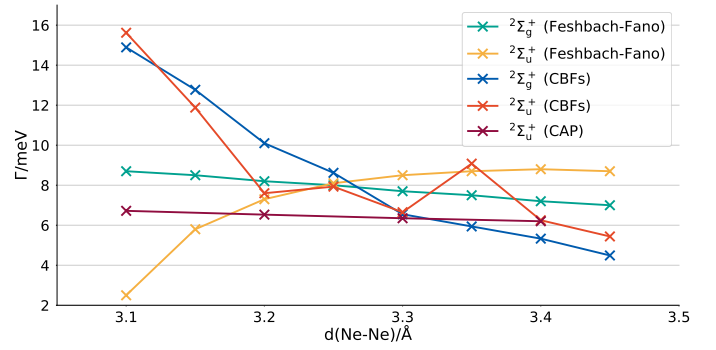


FIG. 4. Total decay width Γ of the two $\text{Ne}_2^+(2s^{-1})$ states as a function of the interatomic distance calculated with CBF-EOM-IP-CCSD/aug-cc-pCVTZ(5sp)+2s2p2d (this work), Feshbach-Fano-EOM-IP-CCSD/aug-cc-pCV5Z (this work) and CAP-EOM-CCSD/aug-cc-pCVTZ (Ref. 12).

tial state and thus not accessible. In Fig. 5, the inner-valence ionization energy is plotted as a function of the interatomic distance (2.0–5.4 Å). It has a very shallow minimum at 2.4 Å and is otherwise almost independent of the interatomic distance, with a value of ca. 48.3 eV. Notably, the equilibrium distances of the neutral and ionized dimers are much larger, 3.5 Å and 3.7 Å, respectively.

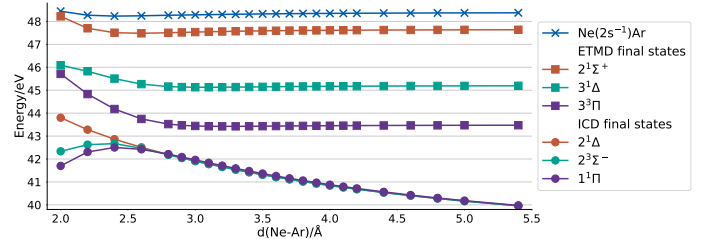


FIG. 5. Selected ionization and double ionization energies of NeAr as a function of the interatomic distance computed with CBF-EOM-IP-CCSD/aug-cc-pCVTZ(5sp)+2s2p2d and EOM-DIP-CCSD/aug-cc-pCVTZ(5sp), respectively. Crosses correspond to the resonance, squares and dots to ETMD and ICD final states, respectively.

We identified 10 ICD target states and 6 ETMD target states. Their EOM-DIP-CCSD energies are reported in Tab. V. Interestingly, all ICD final states are lower in energy than the ETMD target states. This is reflected in the energy of the ejected electron: in the case of ICD, it is around 7 eV for all target states, whereas in the case of ETMD it can assume values between 0.6 eV and 5 eV depending on the target state. Notably, singlet and triplet ICD target states are almost degenerate, while this is not the case for ETMD target states. It is also worth mentioning that the energy of the ICD electrons is one order of magnitude larger for NeAr than for Ne_2 . This is because the target states are more stabilized in the NeAr dimer, owing to the larger energy differences between the orbitals of Ne and Ar. The initial states, on the contrary, have almost the same ionization energies in Ne_2 and NeAr. Our results confirm the ICD electron energy distribution reported in Ref. 63, where the kinetic energy spectra computed for singlet

and triplet states both have a peak in intensity close to 7 eV.

In Fig. 5, selected double ionization energies are reported as a function of the interatomic distance. Results for all states can be found in the Supplementary Material. In the range of distances considered (2.0–5.4 Å) all target states remain accessible via both decay processes, although their relative energy varies. Similar to Ne_2 , the double ionization energies of the ICD target states decrease as the two atoms are moved apart. However, the ICD target states of NeAr all converge to the same energy at large distances, which is not the case for Ne_2 where the states remain parallel to each other.

The energies of the ETMD target states converge to three different values at large distances; in Fig. 5, one state from each group is reported. All double ionization energies corresponding to ETMD target states exhibit a shallow minimum at distances below the equilibrium distance of the ground state (3.5 Å). Since the two charges are on the same atom in the ETMD target states, the interatomic distance does not have a big impact on the double ionization energy, contrary to ICD target states. We note that our results are in agreement with curves that were computed with ADC(2).¹⁵

TABLE V. Selected ionization and double ionization energies of NeAr computed with EOM-CCSD/aug-cc-pCVTZ(5sp)+2s2p2d.

Resonance state	Energy / eV	
$\text{Ne}(2s^{-1})\text{Ar}^+$	48.328	
ICD final states	Singlet / eV	Triplet / eV
1 Δ	41.315	
1 Σ^-		41.315
2 Δ	41.317	
2 Σ^-		41.317
1 Π	41.365	41.362
2 Π	41.469	41.469
1 Σ^+	41.529	41.534
ETMD final states	Singlet / eV	Triplet / eV
2 Σ^+	45.147	
3 Π	45.147	43.433
3 Δ	45.148	
3 Σ^-		43.430
3 Σ^+	47.589	

B. Decay widths

The decay width of Ne^+Ar has been computed several times: with Fano-ADC, a value of 17 meV was determined at the equilibrium distance of neutral NeAr (3.5 Å)⁶³. A previous Fano-ADC treatment resulted in a value of 22 meV,¹⁵ whereas CAP-EOM-CCSD computations delivered a value of 37.4 meV.¹² Also, it has been argued that the ETMD contribution to the width is several orders of magnitude smaller and decays more rapidly with the interatomic distance than the ICD contribution.⁶³

The total widths obtained in our CBF-EOM-IP-CCSD calculations comprises ICD and ETMD contributions. In Fig. 6, we report the values computed at interatomic distances between 2.0 Å and 5.4 Å. We employed in all calculations the

aug-cc-pCVTZ(5sp)+2s2p2d basis set, which yielded the best results for Ne_2^+ . For the neon atom, the exponents of the extra shells are those resulting from the optimization of the $2^2\Sigma_g^+$ state of Ne_2^+ , that is, 0.889 and 0.143, while for argon, two different sets of exponents were employed to check the sensitivity of the method: the results labeled (a) in Fig. 6 were computed using exponents that were obtained from the ones for Ne_2^+ using the procedure described in Sec. II A resulting in values of 0.593 and 0.095. The results labeled (b) in Fig. 6 were obtained with exponents of 0.944 and 0.059 for argon. Since the energy of the outgoing electron does not vary significantly in the range of distances considered here, we can use the same exponents for all internuclear distances.

We find the total decay width of $\text{Ne}(2s^{-1})\text{Ar}^+$ at 3.5 Å to be 15.4 meV with basis set (a) and 18.0 meV with basis set (b), which shows that the width of $\text{Ne}(2s^{-1})\text{Ar}^+$ is much less sensitive to the exponents of the basis functions than that of Ne_2^+ . Notably, our results are in good agreement with Fano-ADC but considerably smaller than the CAP-EOM-CCSD value.

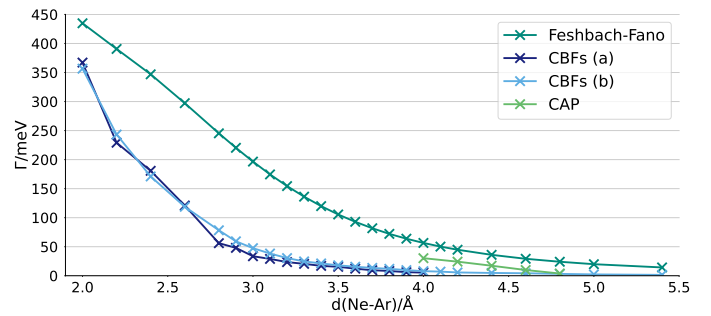


FIG. 6. Total decay width of $\text{Ne}(2s^{-1})\text{Ar}^+$ as a function of the interatomic distance computed with CBF-EOM-CCSD/aug-cc-pCVTZ(5sp)+2s2p2d (this work), Feshbach-Fano-EOM-IP-CCSD/aug-cc-pCV5Z (this work) and CAP-EOM-CCSD/aug-cc-pCVTZ (Ref. 12). The labels (a) and (b) refer to results obtained with different values for the exponents of the complex-scaled shells of the argon atom.

Given that the ETMD width is so much smaller than the ICD width, we do not expect it to have a significant effect on the distance dependence of the total width, meaning we expect $\Gamma(R) \sim R^{-6}$. Our CBF-EOM-IP-CCSD calculations yield $R^{-6.29}$ with basis set (a) and $R^{-5.72}$ with basis set (b). With basis set (a), Γ becomes so small (5.4 meV) beyond 4.0 Å that no minimum can be observed in $d(E_{\text{res}} - E_0)/d\theta$. We therefore re-examined the distance dependence removing the last 5 points, which improved the result to $\Gamma(R) \sim R^{-6.08}$. This might be due to the fact that CBF methods struggle to capture very small widths. Also with basis set (b), $\Gamma(R) \sim R^{-5.99}$ is obtained when the two widths at the shortest distance and the three at the largest distance are not taken into account. With this basis set, the maximum bond length at which a minimum in $d(E_{\text{res}} - E_0)/d\theta$ can be obtained is 5.4 Å, after which the width again becomes too small to be described.

Contrary to the good performance of CBF-EOM-IP-CCSD, the Feshbach-Fano-EOM-CCSD method does not capture the distance dependence of the width of $\text{Ne}(2s^{-1})\text{Ar}^+$ correctly.

As Fig. 6 illustrates, Γ is severely overestimated as compared to CBF-EOM-IP-CCSD. Although the values decrease when the atoms are moved apart, the further analysis yields $\Gamma(R) \sim R^{-3.72}$. This can be slightly improved to $R^{-4.65}$ by only considering values larger than 3.4 Å, but this is still not a satisfactory result.

V. NEON MAGNESIUM DIMER

A. Energetics

As a third example of an atomic dimer, we consider NeMg. As in the case of NeAr, the relaxation of the $2s^{-1}$ vacancy in the neon atom of NeMg can occur both via ICD and ETMD, with the latter process having a width of orders of magnitude smaller than the one of ICD.⁷ The inner-valence ionization energy is ca. 48.3 eV, which is very similar to the previous examples. In Fig. 7, it is plotted as a function of the interatomic distance. The ionization energy exhibits a very shallow minimum at around 3.8 Å, whereas the equilibrium distance of the neutral dimer is 4.4 Å.

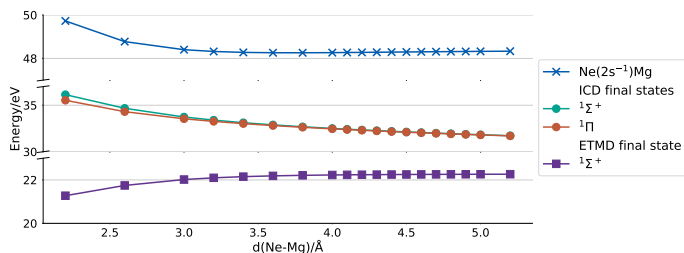


FIG. 7. Selected ionization and double ionization energies of NeMg as a function of the interatomic distance computed with CBF-EOM-IP-CCSD/aug-cc-pCVTZ(5sp)+2s2p2d and EOM-DIP-CCSD/aug-cc-pCVTZ(5sp), respectively. Crosses correspond to the resonance, squares and dots to ETMD and ICD target states, respectively.

For this system, we identified 4 target states accessible via ICD and 1 accessible via ETMD. In Tab. VI, we report their double ionization energies. ICD target states of the type Ne^+Mg^+ are ca. 16 eV lower in energy than the resonance state, which means that the ICD electron has twice as much energy as in the case of NeAr. Singlet and triplet final states are again almost degenerate.

In the case of ETMD, which results in NeMg^{++} , the energy of the outgoing electron is much larger, close to 26 eV. It is interesting to note that, contrary to NeAr, the ETMD final state of NeMg is lower in energy than the ICD final states. This is because the double ionization of the Mg 3s orbital leads to a very stable electronic configuration, which outweighs that the two charges are localized on the same atom. Similar to NeAr, target states of the type Ne^{++}Mg are not accessible because they are too high in energy.

All target states remain accessible at all distances considered here (2.2–5.2 Å). As one can see from Fig. 7, where we report the double ionization energies of the singlet states as a function of the distance, the ICD final states decrease in en-

ergy as the two atoms are moved apart. This is consistent with the trend we observed for Ne_2 and NeAr. The double ionization energy of the ETMD state instead increases with distance, contrary to what we observed for the ETMD final states of NeAr. Also, the double ionization energy of the ETMD state does not exhibit a minimum for the distances considered here. Results for the ICD triplet states can be found in the Supplementary Material.

TABLE VI. Selected ionization and double ionization energies of NeMg computed with EOM-CCSD/aug-cc-pCVTZ(5sp)+2s2p2d.

Resonance state	Energy/eV	
$\text{Ne}(2s^{-1})\text{Mg}^+$	48.291	
ICD final state	Singlet/eV	Triplet/eV
$2 \Sigma^+$	32.198	32.192
1Π	32.169	32.168
ETMD final state	Singlet/eV	Triplet/eV
$1 \Sigma^+$	22.249	

B. Decay widths

The decay width of $\text{Ne}(2s^{-1})\text{Mg}^+$ and its dependence on the interatomic distance has been computed several times.^{7,12,22} In Figure 8, we report CAP-EOM-IP-CCSD results from Ref. 12 alongside our CBF-EOM-IP-CCSD and Feshbach-Fano-EOM-CCSD results. For CBF-EOM-IP-CCSD, the basis set is aug-cc-pCVTZ(5sp)+2s2p2d; the complex exponents for the neon atom are the same that were used for Ne_2 and NeAr, while for the magnesium atom they are obtained by the procedure from Sec. II A. Using the exponents for neon as starting point resulted in exponents of 0.187 and 0.030 for magnesium. Similar to NeAr, we use the same exponents for all distances (2.2–5.2 Å) because the difference between the energy of the resonance and the target-state energies does not change substantially.

CBF-EOM-IP-CCSD delivers the sum of the ICD and ETMD widths although this can be approximated as the ICD width given that the ETMD contribution is very small. At the equilibrium distance of the neutral ground state (4.4 Å), we compute a width of 9.2 meV, which is lower than the CAP-EOM-IP-CCSD value of 17.25 meV reported by Ghosh *et al.*¹² As concerns the distance dependence, CBF-EOM-IP-CCSD yields $\Gamma(R) \sim R^{-5.11}$ meaning that the deviation from the expected result (R^{-6}) is somewhat larger than for NeAr. Contrary to what we saw for NeAr, here the agreement is better at larger distances. When the four points at the shortest distances are removed, we obtain $\Gamma(R) \sim R^{-6.03}$. A possible explanation of the deviation of $\Gamma(R)$ from R^{-6} at short interatomic distances could be that orbital overlap starts playing a significant role, which would make it inappropriate to approximate the full width by the direct ICD contribution.⁷

As concerns Feshbach-Fano-EOM-CCSD, Fig. 8 shows that this method yields larger widths than CBF-EOM-IP-CCSD at all distances considered, in particular at short distances. Moreover, the width does not follow a power law: in

a log-log plot we do not obtain a line but rather a quadratic function. Notably, CAP-EOM-IP-CCSD predicts even larger widths at all interatomic distances reported in Ref. 12 (4.0–4.8 Å). However, the discrepancies between the methods decrease as the atoms are moved apart.

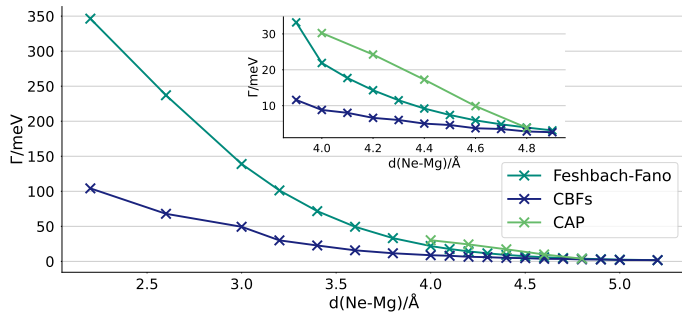


FIG. 8. Total decay width of $\text{Ne}(2s^{-1})\text{Mg}^+$ as a function of the interatomic distance computed with CBF-EOM-CCSD/aug-cc-pCVTZ(5sp)+2s2p2d (this work), Feshbach-Fano-EOM-CCSD/aug-cc-pV5Z (this work), and CAP-EOM-CCSD/aug-cc-pVTZ (Ref. 12).

VI. HYDROGEN FLUORIDE DIMER

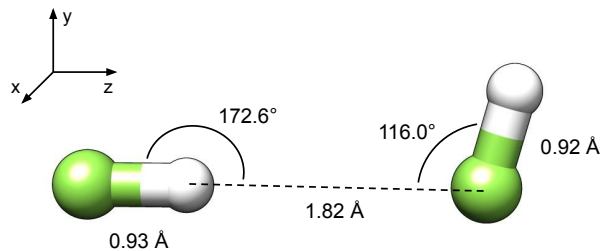


FIG. 9. Optimized structure of $(\text{HF})_2$

As an example of ICD in a molecular system, we computed the decay rate of $(\text{HF})_2$. The optimized structure of this dimer is shown in Fig. 9. This structure was taken from Ref. 64 and re-optimized with RI-MP2/aug-cc-pVTZ; the coordinates are reported in the Supplementary Material. In $(\text{HF})_2$, two distinct resonances result from ionizing the 2s orbitals of the fluorine atoms. They can be distinguished because the vacancies are localized on the fluorine atom of the molecule that acts as H-bond donor or the one that acts as H-bond acceptor. In this work, we focus on the lower-lying state in which the ionized fluorine atom is the one of the H-bond donor, which is shown on the left in Fig. 9.

The inner-valence ionization energy is reported in Tab. VII, while the energies of the accessible target states can be found in Tab. VIII. Our results for the latter states are qualitatively in line with those from Ref. 65 although the energies differ slightly. Notably, the energy of the ICD electron is only 0.3

eV in $(\text{HF})_2^+$, which is much smaller compared to the dimers examined in the previous sections.

Our results for the decay width are reported in Tab. VII. These were computed using the aug-cc-pCVTZ(5sp)+2s2p2d basis, where the exponents of the complex-scaled shells are again obtained by means of the procedure described in Sec. II A using the exponents for Ne_2 as starting point. The values are 0.0915, 0.0057 and 0.985, 0.062 for H and F, respectively. As can be seen from Tab. VII, the resonance positions and widths obtained with CBF-EOM-IP-CCSD are in good agreement with CAP-CI and CAP-EOM-CCSD values available from the literature.^{64,66} For what concerns Feshbach-Fano-EOM-CCSD, however, the total width is one order of magnitude too small, which shows again that the method devised for Auger decay is not suitable to describe ICD.

TABLE VII. Ionization energy and decay width of the lowest resonance state of $(\text{HF})_2^+(2s^{-1})$ computed with various electronic structure methods.

Method	Energy/eV	Width/meV
CBF-EOM-CCSD/aug-cc-pCVTZ(5sp)+2s2p2d (this work)	38.621	17.0
Feshbach-Fano-EOM-CCSD/aug-cc-pV5Z (this work)	39.18	1.8
CAP-CI/aug-cc-pVTZ ⁶⁴	38.6	18.0
CAP-EOM-CCSD/aug-cc-pVTZ ⁶⁶	39.1	20.7

TABLE VIII. Double ionization energies of the states resulting from the decay of $(\text{HF})_2^+(2s^{-1})$ computed with EOM-CCSD/aug-cc-pCVTZ(5sp). Subscripts *d* and *a* refer to the molecule that acts as H-bond donor and acceptor, respectively.

ICD final state	Singlet/eV	Triplet/eV
$\text{HF}_d(2p_x^{-1})\text{HF}_a(2p_x^{-1})$	38.341	38.342
$\text{HF}_d(2p_y^{-1})\text{HF}_a(3p_x^{-1})$	38.345	38.346

VII. DISCUSSION AND CONCLUSIONS

In this work, we investigated interatomic/intermolecular Coulombic decay (ICD) in clusters of atoms and molecules by means of the equation-of-motion coupled-cluster singles and doubles method combined with complex basis functions and, alternatively, Feshbach-Fano projection and a plane wave description for the emitted electron.

In the three atomic dimers Ne_2 , NeAr , and NeMg , the initially ionized orbital is always a neon 2s orbital. Consequently, the ionization energy needed to create the vacancy differs by less than 0.1 eV among the three dimers, whereas the ionized state of $(\text{HF})_2$ is 10 eV lower in energy because the vacancy is in a fluorine 2s orbital.

The energy of the ICD electrons follows a different trend: It assumes values of 0.8 eV for Ne_2 and 0.3 eV for $(\text{HF})_2$ but 7 eV and 16 eV for NeAr and NeMg , respectively. In general,

the energy of the ICD electron is higher when the two participating atoms or molecules are different, as the orbital energy differences are bigger in this case. For the same reason, only the inner-valence vacancies of NeAr and NeMg can relax via electron transfer mediated decay (ETMD). Interestingly, the ETMD electron has a lower energy than the ICD electron in NeAr, while it is larger in the case of NeMg.

To describe ICD and ETMD, complex basis functions offer a framework in which the outgoing electron does not need to be described explicitly. Rather, the decay width is directly obtained from the imaginary part of the total energy. In general, CBF-EOM-IP-CCSD yields results that are in good agreement with previously reported results based on complex absorbing potentials and Fano-Feshbach projection combined with Stieltjes imaging.

However, we found that the performance of CBF-EOM-IP-CCSD is much better for NeAr and NeMg than for Ne₂ and (HF)₂. For the former two systems, the distance dependence of the computed decay widths is in excellent agreement with the expectation, that is, it is proportional to R^{-6} . In contrast, for Ne₂ the distance dependence of the width is less well described. Also, the width of Ne₂ is much more sensitive to changes in the complex-scaled exponents than that of NeAr. We relate both shortcomings to the ICD electron having less energy in Ne₂ as compared to NeAr and NeMg.

Compared to Auger decay, ICD is more difficult to describe with CBF methods. This is not only because the emitted electron is slower but also because ICD widths are typically smaller than Auger decay widths. At their equilibrium structures, the systems considered in this work all have widths between 6 and 17 meV, whereas Auger decay widths can be greater than 100 meV for first-row nuclei and even greater for heavier nuclei. From the analysis of the distance dependence of the widths of NeAr and NeMg, we conclude that values down to ca. 5 meV can be reliably computed with CBF-EOM-IP-CCSD.

Trends in the ICD width among the clusters are influenced by the differences in the interatomic distances and the orbital energies. Notably, the ICD width is very sensitive to a change of the partner atom, while it is almost independent of the energy of the emitted electron, meaning a large decay width does not correspond to a fast electron.

Finally, we note that the Feshbach-Fano approach combined with a plane-wave description for the emitted electron is not suitable to describe ICD. This approach was devised for the treatment of Auger decay where it delivers good results but is unable to capture the characteristic R^{-6} distance dependence of the ICD width. We ascribe this failure to using plane waves as previously reported applications of the Feshbach-Fano approach to ICD relying on Stieltjes imaging yielded convincing results.

SUPPLEMENTARY MATERIAL

Supplementary material is available: geometry of (HF)₂, exponents of Ne₂ as well as double ionization energies and decay widths for all dimers discussed in the article.

ACKNOWLEDGMENTS

T.-C.J. gratefully acknowledges funding from the European Research Council (ERC) under the European Union's Horizon 2020 research and innovation program (Grant Agreement No. 851766) and the KU Leuven internal funds (Grant C14/22/083). We thank Florian Matz and Anthuan Ferino-Pérez for insightful discussions.

AUTHOR DECLARATIONS

Conflict of Interest Statement

The authors have no conflicts to disclose.

Author Contributions

Valentina Parravicini: Conceptualization (equal); Methodology (lead); Investigation (lead); Writing - original draft (lead). **Thomas-C. Jagau:** Conceptualization (equal); Methodology (supporting); Investigation (supporting); Writing - original draft (supporting); Writing review & editing (lead); Funding acquisition (lead).

DATA AVAILABILITY

The data that support the findings of this study are available within the article and its supplementary material.

REFERENCES

- ¹L. S. Cederbaum, J. Zobeley, and F. Tarantelli, "Giant intermolecular decay and fragmentation of clusters," *Phys. Rev. Lett.* **79**, 4778–4781 (1997).
- ²T. Jahnke, U. Hergenhanh, B. Winter, R. Dörner, U. Frühling, P. V. Demekhin, K. Gokhberg, L. S. Cederbaum, A. Ehresmann, A. Knie, and A. Dreuw, "Interatomic and intermolecular Coulombic decay," *Chemical Reviews* **120**, 11295–11369 (2020).
- ³L. Meitner, "Über die β -Strahl-Spektren und ihren Zusammenhang mit der γ -Strahlung," *Z. Phys.* **11**, 35–54 (1922).
- ⁴Auger, "Sur les rayons beta secondaires produits dans un gaz par des rayons x," *C.R.A.S.* **177**, 169–171 (1923).
- ⁵R. Santra, J. Zobeley, and L. Cederbaum, "Electronic decay of valence holes in clusters and condensed matter," *Phys. Rev. B* **64**, 245104 (2001).
- ⁶T. D. Thomas, C. Miron, K. Wiesner, P. Morin, T. X. Carroll, and L. J. Sæthre, "Anomalous natural linewidth in the $2p$ photoelectron spectrum of SiF₄," *Phys. Rev. Lett.* **89**, 223001 (2002).
- ⁷V. Averbukh, I. B. Müller, and L. S. Cederbaum, "Mechanism of interatomic Coulombic decay in clusters," *Phys. Rev. Lett.* **93**, 263002 (2004).
- ⁸T. Miteva, S. Kazandjian, P. Kolorenč, P. Votavová, and N. Sisourat, "Interatomic Coulombic decay mediated by ultrafast superexchange energy transfer," *Phys. Rev. Lett.* **119**, 083403 (2017).
- ⁹P. Votavová, T. Miteva, S. Engin, S. Kazandjian, P. Kolorenč, and N. Sisourat, "Mechanism of superexchange interatomic Coulombic decay in rare-gas clusters," *Phys. Rev. A* **100**, 022706 (2019).
- ¹⁰G. Öhrwall, M. Tchapyguine, M. Lundwall, R. Feifel, H. Bergersen, T. Rander, A. Lindblad, J. Schulz, S. Peredkov, S. Barth, S. Marburger,

- U. Hergenhahn, S. Svensson, and O. Björneholm, "Femtosecond interatomic Coulombic decay in free neon clusters: Large lifetime differences between surface and bulk," *Phys. Rev. Lett.* **93**, 173401 (2004).
- ¹¹S. Barth, S. Marburger, O. Kugeler, V. Ulrich, S. Joshi, A. M. Bradshaw, and U. Hergenhahn, "The efficiency of interatomic Coulombic decay in Ne clusters," *Chem. Phys. Electron Correlation and Multimode Dynamics in Molecules*, **329**, 246–250 (2006).
- ¹²A. Ghosh and N. Vaval, "Geometry-dependent lifetime of interatomic Coulombic decay using equation-of-motion coupled cluster method," *J. Chem. Phys.* **141**, 234108 (2014).
- ¹³E. Fasshauer, "Non-nearest neighbour ICD in clusters," *New J. Phys.* **18**, 043028 (2016).
- ¹⁴R. Kumar, A. Ghosh, and N. Vaval, "Decay processes in cationic alkali metals in microsolvated clusters: A complex absorbing potential based equation-of-motion coupled cluster investigation," *J. Chem. Theory Comput.* **18**, 807–816 (2022).
- ¹⁵J. Zobeley, R. Santra, and L. S. Cederbaum, "Electronic decay in weakly bound heteroclusters: Energy transfer versus electron transfer," *J. Chem. Phys.* **115**, 5076–5088 (2001).
- ¹⁶N. Moiseyev, *Non-Hermitian Quantum Mechanics* (Cambridge University Press, 2011).
- ¹⁷T.-C. Jagau, K. B. Bravaya, and A. I. Krylov, "Extending quantum chemistry of bound states to electronic resonances," *Annu. Rev. Phys. Chem.* **68**, 525–553 (2017).
- ¹⁸T.-C. Jagau, "Theory of electronic resonances: fundamental aspects and recent advances," *Chem. Commun.* **58**, 5205–5224 (2022).
- ¹⁹U. Fano, "Effects of configuration interaction on intensities and phase shifts," *Phys. Rev.* **124**, 1866–1878 (1961).
- ²⁰H. Feshbach, "A unified theory of nuclear reactions. II," *Ann. Phys.* **19**, 287–313 (1962).
- ²¹P. W. Langhoff and C. T. Corcoran, "Stieltjes imaging of photoabsorption and dispersion profiles," *J. Chem. Phys.* **61**, 146–159 (1974).
- ²²V. Averbukh and L. S. Cederbaum, "Ab initio calculation of interatomic decay rates by a combination of the Fano ansatz, Green's-function methods, and the Stieltjes imaging technique," *J. Chem. Phys.* **123**, 204107 (2005).
- ²³P. Kolorenč and V. Averbukh, "Fano-ADC(2,2) method for electronic decay rates," *J. Chem. Phys.* **152**, 214107 (2020).
- ²⁴T. Miteva, S. Kazandjian, and N. Sisourat, "On the computations of decay widths of Fano resonances," *Chem. Phys.* **482**, 208–215 (2017).
- ²⁵N. Sisourat, S. Engin, J. D. Gorfinkiel, S. Kazandjian, P. Kolorenč, and T. Miteva, "On the computations of interatomic Coulombic decay widths with R-matrix method," *J. Chem. Phys.* **146**, 244109 (2017).
- ²⁶R. Santra and L. S. Cederbaum, "An efficient combination of computational techniques for investigating electronic resonance states in molecules," *J. Chem. Phys.* **115**, 6853–6861 (2001).
- ²⁷N. Vaval and L. S. Cederbaum, "Ab initio lifetimes in the interatomic Coulombic decay of neon clusters computed with propagators," *J. Chem. Phys.* **126**, 164110 (2007).
- ²⁸A. Ghosh, S. Pal, and N. Vaval, "Study of interatomic Coulombic decay of $\text{Ne}(\text{H}_2\text{O})_n$ ($n = 1, 3$) clusters using equation-of-motion coupled-cluster method," *J. Chem. Phys.* **139**, 064112 (2013).
- ²⁹W. Skomorowski and A. I. Krylov, "Feshbach-Fano approach for calculation of Auger decay rates using equation-of-motion coupled-cluster wave functions. I. Theory and implementation," *J. Chem. Phys.* **154**, 084124 (2021).
- ³⁰C. W. McCurdy and T. N. Rescigno, "Extension of the method of complex basis functions to molecular resonances," *Phys. Rev. Lett.* **41**, 1364–1368 (1978).
- ³¹J. F. Stanton and R. J. Bartlett, "The equation of motion coupled-cluster method. a systematic biorthogonal approach to molecular excitation energies, transition probabilities, and excited state properties," *J. Chem. Phys.* **98**, 7029–7039 (1993).
- ³²K. Sneskov and O. Christiansen, "Excited state coupled cluster methods," *WIREs: Comp. Mol. Sci.* **2**, 566–584 (2012).
- ³³J. F. Stanton and J. Gauss, "Analytic energy derivatives for ionized states described by the equation-of-motion coupled cluster method," *J. Chem. Phys.* **101**, 8938–8944 (1994).
- ³⁴M. Nooijen and R. J. Bartlett, "A new method for excited states: Similarity transformed equation-of-motion coupled-cluster theory," *J. Chem. Phys.* **106**, 6441–6448 (1997).
- ³⁵K. W. Sattelmeyer, H. F. Schaefer III, and J. F. Stanton, "Use of 2h and 3h-p-like coupled-cluster Tamm-Dancoff approaches for the equilibrium properties of ozone," *Chem. Phys. Lett.* **378**, 42–46 (2003).
- ³⁶C. W. McCurdy, T. N. Rescigno, E. R. Davidson, and J. G. Lauderdale, "Applicability of self-consistent field techniques based on the complex coordinate method to metastable electronic states," *J. Chem. Phys.* **73**, 3268–3273 (1980).
- ³⁷T. N. Rescigno, A. E. Orel, and C. W. McCurdy, "Application of complex coordinate scf techniques to a molecular shape resonance: The $2^2\pi_g$ state of N_2^- ," *J. Chem. Phys.* **73**, 6347–6348 (1980).
- ³⁸M. Honigmann, R. J. Buenker, and H.-P. Liebermann, "Complex self-consistent field and multireference single- and double-excitation configuration interaction calculations for the $2^2\Pi_g$ resonance state of N_2^- ," *J. Chem. Phys.* **125**, 234304 (2006).
- ³⁹M. Honigmann, H.-P. Liebermann, and R. J. Buenker, "Use of complex configuration interaction calculations and the stationary principle for the description of metastable electronic states of HCl^- ," *J. Chem. Phys.* **133**, 044305 (2010).
- ⁴⁰A. F. White, C. W. McCurdy, and M. Head-Gordon, "Restricted and unrestricted non-Hermitian Hartree-Fock: Theory, practical considerations, and applications to metastable molecular anions," *J. Chem. Phys.* **143**, 074103 (2015).
- ⁴¹A. F. White, M. Head-Gordon, and C. W. McCurdy, "Complex basis functions revisited: Implementation with applications to carbon tetrafluoride and aromatic N-containing heterocycles within the static-exchange approximation," *J. Chem. Phys.* **142**, 054103 (2015).
- ⁴²A. F. White, E. Epifanovsky, C. W. McCurdy, and M. Head-Gordon, "Second order Møller-Plesset and coupled cluster singles and doubles methods with complex basis functions for resonances in electron-molecule scattering," *J. Chem. Phys.* **146**, 234107 (2017).
- ⁴³T.-C. Jagau, "Coupled-cluster treatment of molecular strong-field ionization," *J. Chem. Phys.* **148**, 204102 (2018).
- ⁴⁴M. Hernández Vera and T.-C. Jagau, "Resolution-of-the-identity approximation for complex-scaled basis functions," *J. Chem. Phys.* **151**, 111101 (2019).
- ⁴⁵M. Hernández Vera and T.-C. Jagau, "Resolution-of-the-identity second-order Møller-Plesset perturbation theory with complex basis functions: Benchmark calculations and applications to strong-field ionization of polyacenes," *J. Chem. Phys.* **152**, 174103 (2020).
- ⁴⁶T. H. Thompson, C. Ochsenfeld, and T.-C. Jagau, "A schwarz inequality for complex basis function methods in non-hermitian quantum chemistry," *J. Chem. Phys.* **151**, 184104 (2019).
- ⁴⁷F. Matz and T.-C. Jagau, "Molecular Auger decay rates from complex-variable coupled-cluster theory," *J. Chem. Phys.* **156**, 114117 (2022).
- ⁴⁸F. Matz and T.-C. Jagau, "Channel-specific core-valence projectors for determining partial Auger decay widths," *Mol. Phys.* **120**, e2105270 (2022).
- ⁴⁹N. K. Jayadev, A. Ferino-Pérez, F. Matz, A. I. Krylov, and T.-C. Jagau, "The Auger spectrum of benzene," *J. Chem. Phys.* **158**, 064109 (2023).
- ⁵⁰W. Skomorowski and A. I. Krylov, "Feshbach-Fano approach for calculation of Auger decay rates using equation-of-motion coupled-cluster wave functions. II. Numerical examples and benchmarks," *J. Chem. Phys.* **154**, 084125 (2021).
- ⁵¹J. Aguilar and J. M. Combes, "A class of analytic perturbations for one-body Schrödinger Hamiltonians," *Commun. Math. Phys.* **22**, 269–279 (1971).
- ⁵²E. Balslev and J. M. Combes, "Spectral properties of many-body Schrödinger operators with dilatation-analytic interactions," *Commun. Math. Phys.* **22**, 280–294 (1971).
- ⁵³A. T. B. Gilbert, N. A. Besley, and P. M. W. Gill, "Self-consistent field calculations of excited states using the maximum overlap method (MOM)," *J. Phys. Chem. A* **112**, 13164–13171 (2008).
- ⁵⁴N. Moiseyev, P. Certain, and F. Weinhold, "Resonance properties of complex-rotated hamiltonians," *Mol. Phys.* **36**, 1613–1630 (1978).
- ⁵⁵E. Epifanovsky, A. T. B. Gilbert, X. Feng, J. Lee, Y. Mao, N. Mardirossian, P. Pokhilkov, A. F. White, M. P. Coons, A. L. Dempwolff, Z. Gan, D. Hait, P. R. Horn, L. D. Jacobson, I. Kaliman, J. Kussmann, A. W. Lange, K. U. Lao, D. S. Levine, J. Liu, S. C. McKenzie, A. F. Morrison, K. D. Nanda, F. Plasser, D. R. Rehn, M. L. Vidal, Z.-Q. You, Y. Zhu, B. Alam, B. J. Albrecht, A. Aldossary, E. Alguire, J. H. Andersen, V. Athavale, D. Barton, K. Begam, A. Behn, N. Bellonzi, Y. A. Bernard, E. J. Berquist,

- H. G. A. Burton, A. Carreras, K. Carter-Fenk, R. Chakraborty, A. D. Chien, K. D. Closser, V. Cofer-Shabica, S. Dasgupta, M. de Wergifosse, J. Deng, M. Diedenhofen, H. Do, S. Ehlert, P.-T. Fang, S. Fatehi, Q. Feng, T. Friedhoff, J. Gayvert, Q. Ge, G. Gidofalvi, M. Goldey, J. Gomes, C. E. González-Espinoza, S. Gulania, A. O. Gunina, M. W. D. Hanson-Heine, P. H. P. Harbach, A. Hauser, M. F. Herbst, M. Hernández Vera, M. Hodecker, Z. C. Holden, S. Houck, X. Huang, K. Hui, B. C. Huynh, M. Ivanov, Á. Jász, H. Ji, H. Jiang, B. Kaduk, S. Kähler, K. Khistyayev, J. Kim, G. Kis, P. Klunzinger, Z. Koczor-Benda, J. H. Koh, D. Kosenkov, L. Koulias, T. Kowalczyk, C. M. Krauter, K. Kue, A. Kunitsa, T. Kus, I. Ladjászki, A. Landau, K. V. Lawler, D. Lefrançois, S. Lehtola, R. R. Li, Y.-P. Li, J. Liang, M. Liebenthal, H.-H. Lin, Y.-S. Lin, F. Liu, K.-Y. Liu, M. Loipersberger, A. Luenser, A. Manjanath, P. Manohar, E. Mansoor, S. F. Manzer, S.-P. Mao, A. V. Marenich, T. Markovich, S. Mason, S. A. Maurer, P. F. McLaughlin, M. F. S. J. Menger, J.-M. Mewes, S. A. Mewes, P. Morgante, J. W. Mullinax, K. J. Oosterbaan, G. Paran, A. C. Paul, S. K. Paul, F. Pavošević, Z. Pei, S. Prager, E. I. Proynov, Á. Rák, E. Ramos-Cordoba, B. Rana, A. E. Rask, A. Rettig, R. M. Richard, F. Rob, E. Rossomme, T. Scheele, M. Scheurer, M. Schneider, N. Sergueev, S. M. Sharada, W. Skomorowski, D. W. Small, C. J. Stein, Y.-C. Su, E. J. Sundstrom, Z. Tao, J. Thirman, G. J. Tornai, T. Tsuchimochi, N. M. Tubman, S. P. Veccham, O. Vydrov, J. Wenzel, J. Witte, A. Yamada, K. Yao, S. Yeganeh, S. R. Yost, A. Zech, I. Y. Zhang, X. Zhang, Y. Zhang, D. Zuev, A. Aspuru-Guzik, A. T. Bell, N. A. Besley, K. B. Bravaya, B. R. Brooks, D. Casanova, J.-D. Chai, S. Coriani, C. J. Cramer, G. Cserey, A. E. DePrince, R. A. DiStasio, A. Dreuw, B. D. Dunietz, T. R. Furlani, W. A. Goddard, S. Hammes-Schiffer, T. Head-Gordon, W. J. Hehre, C.-P. Hsu, T.-C. Jagau, Y. Jung, A. Klamt, J. Kong, D. S. Lambrecht, W. Liang, N. J. Mayhall, C. W. McCurdy, J. B. Neaton, C. Ochsenfeld, J. A. Parkhill, R. Peverati, V. A. Rassolov, Y. Shao, L. V. Slipchenko, T. Stauch, R. P. Steele, J. E. Subotnik, A. J. W. Thom, A. Tkatchenko, D. G. Truhlar, T. Van Voorhis, T. A. Wesolowski, K. B. Whaley, H. L. Woodcock, P. M. Zimmerman, S. Faraji, P. M. W. Gill, M. Head-Gordon, J. M. Herbert, and A. I. Krylov, "Software for the frontiers of quantum chemistry: An overview of developments in the Q-Chem 5 package," *J. Chem. Phys.* **155**, 084801 (2021).
- ⁵⁶D. Zuev, T.-C. Jagau, K. B. Bravaya, E. Epifanovsky, Y. Shao, E. Sundstrom, M. Head-Gordon, and A. I. Krylov, "Complex absorbing potentials within EOM-CC family of methods: Theory, implementation, and benchmarks," *J. Chem. Phys.* **141**, 024102 (2014).
- ⁵⁷L. S. Cederbaum, W. Domcke, and J. Schirmer, "Many-body theory of core holes," *Phys. Rev. A* **22**, 206–222 (1980).
- ⁵⁸S. Coriani and H. Koch, "Communication: X-ray absorption spectra and core-ionization potentials within a core-valence separated coupled cluster framework," *J. Chem. Phys.* **143**, 181103 (2015).
- ⁵⁹M. L. Vidal, X. Feng, E. Epifanovsky, A. I. Krylov, and S. Coriani, "New and efficient equation-of-motion coupled-cluster framework for core-excited and core-ionized states," *J. Chem. Theory Comput.* **15**, 3117–3133 (2019).
- ⁶⁰S. Scheit, V. Averbukh, H.-D. Meyer, N. Moiseyev, R. Santra, T. Sommerfeld, J. Zobeley, and L. S. Cederbaum, "On the interatomic Coulombic decay in the Ne dimer," *J. Chem. Phys.* **121**, 8393–8398 (2004).
- ⁶¹T. Jahnke, A. Czasch, M. S. Schöffler, S. Schössler, A. Knapp, M. Käs, J. Titze, C. Wimmer, K. Kreidi, R. E. Grisenti, A. Staudte, O. Jagutzki, U. Hergenhahn, H. Schmidt-Böcking, and R. Dörner, "Experimental observation of interatomic Coulombic decay in neon dimers," *Phys. Rev. Lett.* **93**, 163401 (2004).
- ⁶²K. Schnorr, A. Senftleben, M. Kurka, A. Rudenko, L. Foucar, G. Schmid, A. Broska, T. Pfeifer, K. Meyer, D. Anielski, R. Boll, D. Rolles, M. Kübel, M. F. Kling, Y. H. Jiang, S. Mondal, T. Tachibana, K. Ueda, T. Marchenko, M. Simon, G. Brenner, R. Treusch, S. Scheit, V. Averbukh, J. Ullrich, C. D. Schröter, and R. Moshhammer, "Time-resolved measurement of interatomic Coulombic decay in Ne₂," *Phys. Rev. Lett.* **111**, 093402 (2013).
- ⁶³S. Scheit, V. Averbukh, H.-D. Meyer, J. Zobeley, and L. S. Cederbaum, "Interatomic Coulombic decay in a heteroatomic rare gas cluster," *J. Chem. Phys.* **124**, 154305 (2006).
- ⁶⁴R. Santra, L. S. Cederbaum, and H. D. Meyer, "Electronic decay of molecular clusters: non-stationary states computed by standard quantum chemistry methods," *Chem. Phys. Lett.* **303**, 413–419 (1999).
- ⁶⁵J. Zobeley, L. S. Cederbaum, and F. Tarantelli, "Highly excited electronic states of molecular clusters and their decay," *J. Chem. Phys.* **108**, 9737–9750 (1998).
- ⁶⁶A. Ghosh, S. Pal, and N. Vaval, "Interatomic Coulombic decay in HF_n (n = 2–3) clusters using CAP/EOM-CCSD method," *Mol. Phys.* **112**, 669–673 (2014).